Research Article

Journal of RAMAN SPECTROSCOPY

Received: 11 February 2009 Accepted: 20 May 2009 Published online in Wiley Interscience: 31 July 2009

(www.interscience.wiley.com) DOI 10.1002/jrs.2366

Nano-scale analysis of graphene layers by tip-enhanced near-field Raman spectroscopy

Yuika Saito,[a] Prabhat Verma,[b,c*] Kyoko Masui,[c] Yasushi Inouye[b] and Satoshi Kawata[c]

We demonstrate nano-scale optical analysis of graphene layers by tip-enhanced near-field Raman spectroscopy (TERS). In this technique, the spatial resolution ~30 nm is realized by the near-field probe which acts as a nano-light source. From the intensity change of the Raman band of silicon generated from the near-field probe, we can conveniently estimate the edge boundaries and the number of stacking layers. TERS measurement across the layer edges reveals the nano-scale properties of the material as well as the existence of local defects and edge boundaries. The intensity change of the G-band shows the step-like behavior that follows the layer boundary, whereas the two components in 2D peak show more complex behaviors even inside layers. The peak fluctuation in the 2D band also suggests the local stress distribution due to interlayer interactions. An excess charge effect is observed through the correlation between the peak position and the width of the G-band and their nano-scale distribution within a layer is revealed. Besides the vibrational analysis, we successfully performed the estimation of the number of layers in two-dimensional imaging by the same experimental platform, which allows us high-throughput nondestructive identification of graphene layers critical for the evaluation of this material especially in future device applications.

Keywords: near-field; apertureless probe; tip-enhanced Raman spectroscopy; graphite; graphene

Introduction

Since the synthetic breakthrough of graphene, which is a single layer of graphite, in 2005, the material has attracted significant attention both in the field of basic science and in device applications.[1,2] The importance of graphene can be dominantly attributed to its anomalous electronic properties. The electron transport in graphene is described by the Dirac formulation that allows access to quantum electrodynamics in a simple condensed matter experiment.[3,4] Extraordinary features of this material, such as ballistic transport at room temperature combined with chemical and mechanical stabilities, make it a promising candidate for its applications in devices in nano-dimensions.[5] Recently, a bottom gate modulation of the current in the plane of a graphene film with *n* layers (*n*-graphene) was demonstrated, which represented for the first time that gate control of current could be observed in a metallic or semimetallic system.[6] The other important reason for the popularity of the material is that various forms of carbon families such as graphite, carbon nanotubes, buckyballs, and others can all be viewed as derivatives of graphene. Phonon and electron dispersions in graphene have been studied theoretically for many years.[7] In fact, these dispersion curves led to the prediction of chirality-dependent one-dimensional electron and phonon dispersions in carbon nanotubes, which has been widely studied in the recent years. The study of graphene at last allows us to probe it experimentally, which paves the way to better understanding the other carbon families.[8]

Graphite has isotropic structure in two dimensions; however, a periodic ABAB stacking of graphene layers in the third dimension makes it a strongly anisotropic layered material. The entire formal chemical bonding in graphite is associated with strong sp^2 intralayer bonds, while the interlayer interactions are only weak van der Waals bonds. However, by employing optical spectroscopic method, despite the short range and weak interlayer forces within these films, surprisingly continuous and systematic changes in the first- and second-order high wavenumber interlayer phonon were observed as the number of layer *n* increased.[9] Spectroscopic methods can therefore be used to identify the number of layers, as well as to study the electronic and vibrational properties of the material in an *n*-graphene. In comparison with electron microscopy and scanning probe microscopy, vibrational spectroscopy such as Raman spectroscopy that targets vibrational energy analysis, focuses more on structural information, such as intermolecular interactions, molecular orientations, and symmetry distortions of each species. The conventional confocal Raman spectroscopy technique is limited to subwavelength spatial resolution, and hence localized vibrational features of materials at nano-scale cannot be resolved. This limitation has been overcome by the development of tip-enhanced Raman spectroscopy (TERS).[10,11]

* *Correspondence to: Prabhat Verma, Graduate School of Frontier Biosciences, Osaka University, Suita, Osaka, 565-0871 Japan. E-mail: verma@ap.eng.osaka-u.ac.jp*

a *Frontier Research Center, Osaka University, 2-1 Yamadaoka, Suita, Osaka, 565-0871 Japan*

b *Graduate School of Frontier Biosciences, Osaka University, Suita, Osaka, 565-0871 Japan*

c *Department of Applied Physics, Osaka University, Suita, Osaka, 565-0871 Japan*

Journal of RAMAN SPECTROSCOPY

By introducing a sharp metallic nano-tip to the focus of a laser beam, one can effectively collect localized Raman scattering from an area of ~30 nm^2.[12–14] This technique has recently been successfully applied to other carbon families, especially to single walled carbon nanotubes (SWNTs). The molecular nanoimaging, photoluminescence mapping, and chirality evaluations of SWNTs have been performed by this method.[15–17] Furthermore, the stress effect on SWNTs has been studied under TERS measurement, which revealed that specific Raman bands show significant shifts when the sample is uniaxially pressurized by the apex of a nano-tip.[18] Similar effect has also been observed in the case of C_{60}.[19] One can easily find a correlation of these works to the stress effects on graphene bandgaps.[20]

In this report, we present TERS analysis of *n*-graphene, where $3 \leq n \leq 6$. Continuous change of intensity and peak shift of the well-known graphite mode (G-band) and the second-order overtone of the defect mode (2D-band) across the layer boundaries were observed. The results offer a unique characteristic of the sample in nano-scale resolution. Apart from observing Raman scattering from the graphene layers, we also provide another convenient near-field optical method for the estimation of the layer number *n* under the same experimental platform and demonstrate a high-resolution two-dimensional imaging of thickness distribution in ultrathin graphite flakes. In this method, instead of observing Raman scattering from graphene, we observed the transmission of Raman scattering of silicon through the graphene sample. Since absorption in graphene is more prominent than Raman scattering, this method provides optical nanoimage with high contrast that is suitable for ultrathin sample with just a few layers of graphene. We are able to identify the exact number of layers in ultrathin sample with a high spatial resolution of about 20 nm.

Experimental

A schematic view of our experimental apparatus is shown in Fig. 1. The system is an inverted-microscope-based transmission mode setup. Laser excitation was provided by low power of a continuous-wave argon ion laser ($\lambda = 514$ nm). The beam was expanded 20 folds using a beam expander, and a beam-shaping mask was inserted into the excitation beam path to generate a purely evanescent field at the surface of a cover slip, on which the sample was placed. The excitation beam was focused through an inverted oil-immersion microscope objective lens (×60, NA = 1.4), and Raman signal was efficiently collected by the same. A pinhole with a diameter of 200 m was inserted in the output of the microscope to effectively reject the far-field background. The signal was guided to a single spectrometer and detected using a liquid-nitrogen-cooled charge coupled device (CCD) camera set at an exposure time of 20 s at each point. More details of the present experimental setup can be found elsewhere.[21]

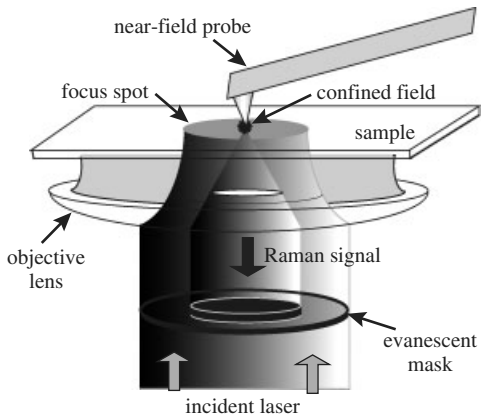

Figure 1. A schematic illustration of the experimental setup used in the present study.

The near-field and the far-field TERS experiments were performed by bringing a silver-coated tip close to the sample, and by taking it away, respectively. Line scan measurements were performed at nanometric resolution. The nano-tip used for these experiments was prepared from commercially available silicon cantilever used in atomic force microscopy (AFM), by coating it with 40-nm-thick silver layer under vacuum evaporation at the rate of 0.5 Å/s. The size of the tip apex after silver coating was about 30 nm, as confirmed from a scanning electron microscope (SEM) image of the tip apex.

Two-dimensional imaging was performed basically with the same experimental platform, by employing an *x*-*y* scanning mode. The near-field probe in this case was a normal silicon AFM tip, which, unlike the previous experiment, was not coated with silver. Near-field measurements were performed at the exposure of 20 s, and the image was obtained from the sample area of 1.2 m ×1.2 m, with a resolution of 64 square pixels scanned at the steps of 20 nm. After the near-field imaging, an AFM image from the same area was obtained at a higher resolution of 256 square pixels using the same tip to confirm the topography of the sample.

A highly oriented pyrolytic graphite (HOPG) foil was purchased from Wako Chemical Co. Ultrathin layers of graphite flakes on a cover slip were prepared by scotch tape cleavage.[22] The graphite sample was cleaved 15 times by a scotch mending tape, which was then rubbed on a glass cover slip for its better fixing. To increase the adhesion force between graphite and the substrate, the cover slip was cleaned in advance in a mixture of boiling HCl and H_2O_2 solution for 20 min, followed by rinsing in distilled water. The sample area with ultrathin graphite ($n < 10$) was still too little in comparison with the thicker graphite flakes. Therefore, we carefully selected a suitable graphite flake on the cover slip by investigating it under an optical microscope equipped with a CCD camera, and used this flake as the sample for further studies.

Results and Discussion

TERS of ultrathin graphite across the layers

We measured TERS across the edge boundaries of graphene layers to investigate the vibrational and electronic properties in nano-scale spatial resolution. Figure 2 (a) shows an optical image of the graphene layers, where some of the edge boundaries can be visibly seen. The graphite area appears dark while the glass substrate appears relatively brighter under the optical microscope. TERS measurements were performed from the thicker to thinner area along the arrow illustrated in Fig. 2(a), which are presented as a waterfall picture in Fig. 2(b). The *x*-axis indicates wavenumbers ranging from 1000 to 3000 cm^{-1}, the *y*-axis corresponds to the tip positions during the measurements at 56 points along the arrow, and the *z*-axis shows Raman intensity. Figure 2(c) shows a typical TERS spectrum from this sample, the main Raman features in which are a weak D-band, a sharp G-band, and a multipeak 2D-band. The assignment of the D-band, which appears around 1360 cm^{-1}, has undergone a debate that has lasted several decades. The

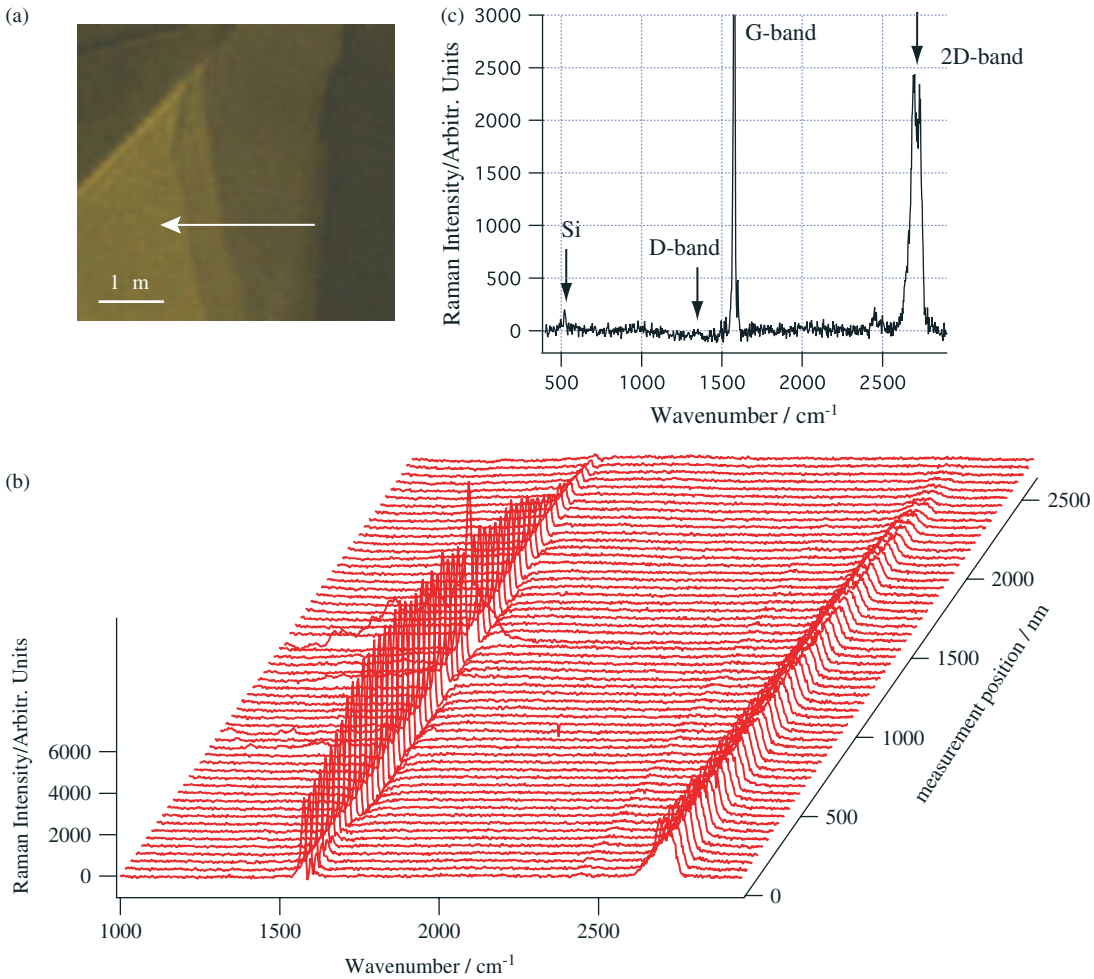

Figure 2. (a) An optical image of ultrathin graphene sample prepared on a glass cover slip, showing the edge boundaries. The brighter areas indicate glass cover slip or very thin sample layers, while the darker areas denote comparatively thicker layers. (b) TERS measurements were performed across the edge boundaries at 56 points separated at nanometric distances, along the arrow shown in the optical image. The spectra are shown as a waterfall picture to emphasize their spatial variations. (c) The magnified view of a typical TERS spectrum taken from the waterfall picture.

recent understanding is that this mode arises from the so-called double resonance (DR) process where Raman scattering is a fourth-order process involving four virtual transitions including phonons, defects, electrons, and holes.[23–24] It is common for graphene not to have enough structural defects for the D-band to be Raman active, so that it can only be seen at the edges. An increased intensity of this mode can therefore be a good signature of the edge boundary. The G-band appears at about 1580 cm^{-1}, the origin of which is the bond stretching of all pairs of sp^2-bonded atoms.[25] The other prominent feature in graphene, the 2D-band, lies around 2700 cm^{-1} and is always seen even when no first-order D-mode is present, since the selection rules do not require defects to be present for the activation of second-order phonons.[3] Apart from all these vibrational modes from the sample, one can always observe a silicon peak at 520 cm^{-1}, which originates from the material of the tip.

Figure 2(b) indicates a gradual decrease in Raman intensity from graphene layers toward the glass surface. However, in the middle of the waterfall picture, a spectrum with a distinguished G-band is observed. From the view of the spectrum, we recognize that it is not the intensity of G-band that increases but the D-band that shows a significant broadening and a huge enhancement. The sudden appearance of this strong D-band could be invoked by either a layer edge or a local defect. It has been reported that the intensity of the D-band depends on the type of an edge; it is stronger at armchair edges and weaker at zigzag edges.[26] However, in both cases, the spectral shape is not as broad as in this case. So, this broad-range enhancement of the D-mode is more likely due to some highly localized defect underneath the near-field probe at that particular position. The reason for the huge enhancement and to what extent the interaction between the surface plasmon of the probe and the graphitic electron causes the spectral change is still uncertain. More experimental data on defects should be collected to reveal the origin of this finding. We omit this particular spectrum in our further discussion.

Figure 3 illustrates the integrated peak intensity of each Raman modes along the spatial positions. The position dependences of TERS intensity of the silicon peak from the probe, of the D-band, the G-band and the 2D-band are shown in Figs 3(a)–3(d), respectively. It is known that the layer number n in a graphene sheet can be distinguished from the spectral shape of the 2D-band.[9] However, in actual data, it is not easy to distinguish the difference between $3 \leq n \leq 10$, though it is possible to determine $n = 1, 2$ and $n = \infty$. We can also determine n directly by AFM; however, the thickness of one graphene layer is so small (0.355 nm) that precise calibration with many number of repeated experiments are necessary.[27] We

Journal of RAMAN SPECTROSCOPY

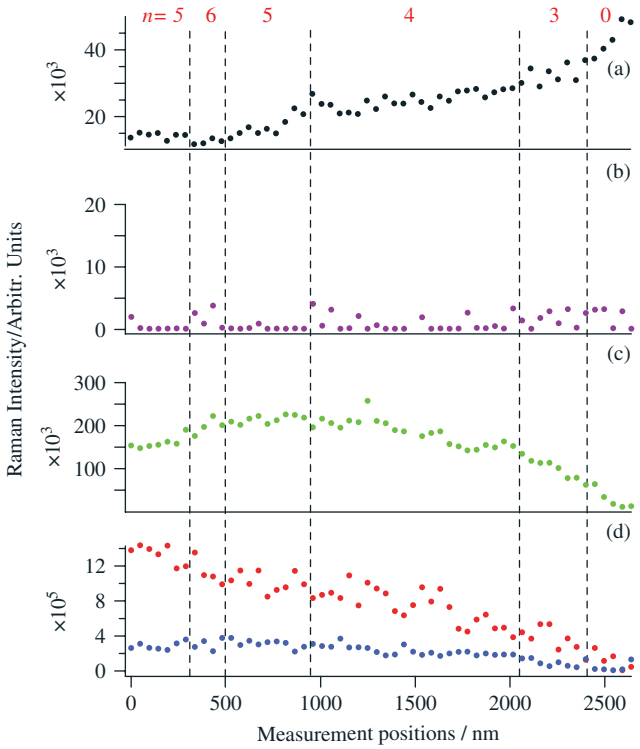

Figure 3. Spatial variations of integrated intensities of Raman bands across the layer boundaries obtained by TERS are plotted. The intensities of silicon mode at 520 cm^{-1}, originating form the tip material, are shown in (a). TERS intensities of the D-band, the G-band, and the two components of 2D-band are shown in (b), (c) and (d), respectively. Red circles correspond to $2D_1$ and blue circles correspond to $2D_2$ mode in (d). The vertical dotted lines indicate layer boundaries, estimated from the variation in the intensity of silicon mode. The estimated numbers of layers are also indicated.

therefore took another approach to determine the layer edge boundaries from the data shown in Figs 3(a) and 3(b). Figure 3(a) tentatively shows stepwise decrease of the silicon peak intensity. The decrease of the silicon peak is caused by the absorption of the scattered light by the sample, which lies between the silicon probe tip and the detection system. The strongest signal is obtained when the probe is on the glass substrate and the signal becomes weaker as the probe comes over the thicker part of the sample. On the basis of this assumption, we estimate the layer boundaries as shown by the dotted lines in Fig. 3 and the layer numbers are estimated as $n = 5, 6, 5, 4, 3$ from the left to right. The number of graphene layers was estimated from the amount of decrease in average intensity of the Raman peak. More description about the estimations of these numbers will be provided later in this article. Ignoring the thinnest area, slight increase of the D-band intensity in Fig. 3(b) at the dotted lines is also consistent with the assignment of the layer edge boundaries. Some small additional fluctuations of D-band intensity could be due to occasional defects in the sample.

Figure 3(c) shows the position dependence of the intensity of the G-band. The step-like response can be seen at several points on the boundary, though it is less clear compared to the silicon band in Fig. 3(a). The intensity of the G-band should, in principle, follow the layer thickness; however, it is not exactly proportional to the layer number *n*. Since this mode is much stronger compared to other modes, it is possible that small changes due to the variation of a small number of layers are buried under the strong intensity and are not clearly visible in the experiment. Because of this reason, Raman imaging through G-band would not show any clear edge boundary, as it does not show any definite dependence on the layer number.

Figure 3(d) illustrates the peak intensity change of the 2D-band. In a monolayer of graphene, the 2D-band appears as a single sharp peak, while in a bilayer, the interaction of the graphene planes causes the π and π^* bands to divide in four bands, the resulting Raman spectra appears as four components.[28] The two-peak shape of the 2D-band in the Raman spectrum of bulk graphite is caused by the convolution of an infinite number of peaks.[25] In this paper, we tentatively decomposed the 2D-band into two component $2D_1$ (lower wavenumber component) and $2D_2$ (higher wavenumber component) to avoid complexity. They are shown by the red and the blue circles, respectively, in Fig. 3(d). In the case of the TERS spectral analysis, the $2D_1$ is always dominant throughout the measurement area. It is certain that the $2D_1$ component includes surface modes of graphite; however, instead of showing a stepwise intensity variation, it rather shows an almost smooth variation in intensity with a number of layers, without showing a clear variation at the edge boundaries. Thus, this mode is also disqualified for Raman imaging that can potentially image layer edge boundaries. On the other hand, the $2D_2$ component is quite weak and hardly shows any clear variation of intensity with layer thickness, and vanishes completely when $n = 3$ or less, indicating that this mode can be attributed to an underlayer component. Considering the origin of the 2D-band, which consists of four or more components due to the DR effect linked with the phonon wave vector to the electronic band structures, the intensity fluctuation may be caused by the interlayer interactions of the week electrostatic forces between layers, which could be easily affected by the layer stacking conditions.

Apart from the intensity variation, the TERS spectra also show some shifts in the Raman modes that depend on the number of layers. Figure 4(a)–(d) shows the spatial dependence of peak positions for the silicon peak, the G-band, the $2D_1$-band and the $2D_2$-band, respectively. As shown in Fig. 4(a), the position of the silicon peak fluctuates within ± 1 cm^{-1}, while its average value remains around 520 cm^{-1}, supporting the accuracy of the measurement. The peak position of the G-band shows slight shift, particularly towards thicker layers. An earlier report showed that the G-band was downshifted with increasing layer number *n*.[9] This shift was usually larger ($\sim$5 or 6 cm^{-1}) from monolayer to bilayer, and smaller ($<$2 cm^{-1}) from bilayer to bulk. The *n* dependence of the shift in the G-band was connected to the strain that arises due to the coupling to the substrate or to the other stacking layers. In our experiment, however, we could see only a slight shift as the layer number *n* increased. In another study, Casiraghi *et al*. observed strong variation in the Raman spectra for various single-layer graphene samples obtained by micromechanical cleavage, and noted the existence of excess charges, even in the absence of intentional doping.[29–30] The peak shift was usually larger than that due to the layer stacking effect. Excess charges can be due to substrate, adsorbents, or are unintentionally incorporated during the process of sample preparations. Interestingly, the downshift in the G-band caused by the access of charge is also accompanied with an increase in the linewidth. Figure 5 shows the variation of linewidth with respect to the peak position for the G-band. Though there is a large fluctuation in Fig. 5, it still confirms a tendency that the linewidth increases with the downshift of the G-band peak position. This is similar to what was earlier reported[31] and also

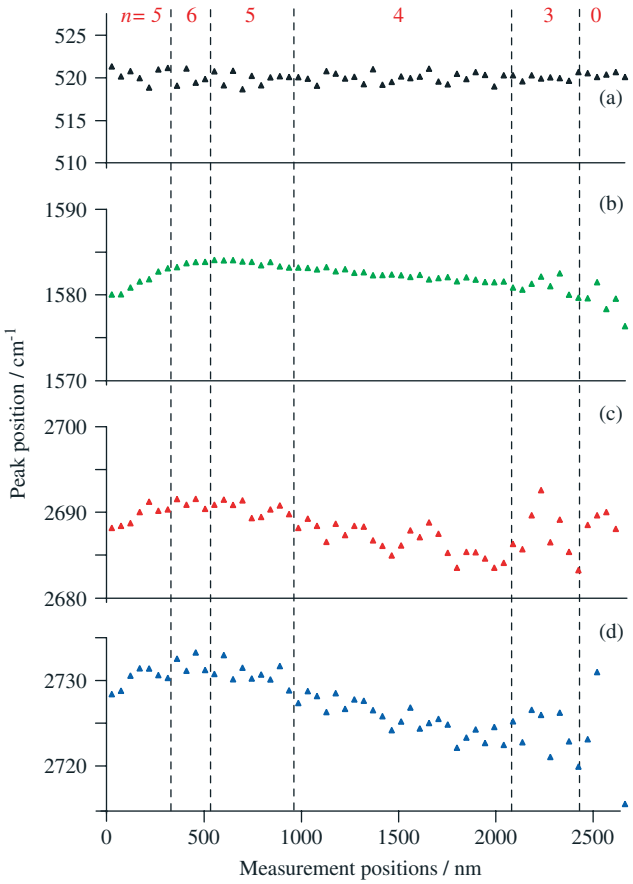

Figure 4. Spatial variations of the peak positions of Raman bands across the layer boundaries are plotted. The peak positions of silicon mode, originating from the tip material and the peak positions of the G-band are shown in (a) and (b), respectively. The spatial variations of the $2D_1$ and $2D_2$ components of the 2D-band are shown in (c) and (d), respectively.

consistent with the result of intentionally doped graphene where the Fermi energy was modulated using a gate.[32]

The peak positions of the two components in the 2D-band show fluctuations even within the same layer. It is known that the 2D-band exhibits a dramatic change of shape with *n*. While four or more spectral components are necessary for precise analysis of this Raman band, only two are employed for our spectral analysis. However, we can still discuss that the shifts in the peak positions of these two components of the 2D-band can be indicators of the interlayer interactions of *n*-graphene sheet. As Fig. 4(c) and (d) suggests, the wavenumbers of both $2D_1$ and $2D_2$ modes become lower at the layer edges and higher in the middle of the layers, especially for the thinner layers in the spatial position of 2000–2300 nm. Since the wavenumber position of a Raman mode is always very sensitive to the local strain,[32] this tendency suggests an inhomogeneous distribution of the strain inside the layer. To evaluate the details of the strain effect via interlayer interactions, it will be promising to observe low wavenumber phonons ($<100\ cm^{-1}$) which are directly connected to the interlayer modes,[33] though it is impossible in the present experimental system. The overall behavior of the peak shift for both $2D_1$ and $2D_2$ bands shows a similar tendency as the G-band, which can also be attributed to the charge effect described before.

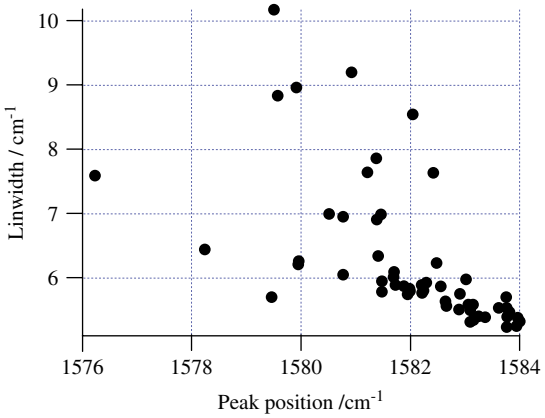

Figure 5. A correlation between the peak position and the line width half-width at half-maxima (HWHM) of the G-band at different positions is plotted, which shows a tendency of increasing line width with downshift of the mode, in agreement with the excess charge effect.

Two-dimensional imaging and estimation of the number of layers

During the TERS measurements, we noticed that none of the Raman modes from graphene showed any clear dependence on either layer number or edge boundaries so that they could possibly be used to construct a high-contrast Raman image to identify graphene layers in the sample. On the other hand, the intensity decrease of the silicon Raman signal from the silicon tip was proportional to the layer number *n* and it also showed a step-like behavior at the edge boundaries. This is because in our measurement of Raman scattering originating from the silicon tip, both the incident laser and the Raman scattering signal pass through the highly absorbent graphene sample (Fig. 1), which has almost constant absorption response in the visible range.[34] We therefore utilized this decrease of Raman signal to construct a near-field optical image that could clearly show graphene layers and the edge boundaries. In a typical TERS experiment, the light field is confined and enhanced at the apex of a metal-coated silicon nano-tip, resulting from the resonant oscillations of the localized surface plasmon polaritons in the thin metallic layer. However, even if a silicon nano-tip is used without metal coating, a strong confinement of light at the apex of the tip can be obtained, which is essentially due to the dipole creation and interaction in silicon by the excitation laser. In this case, however, the enhancement of the field is much weaker than the previous case. In order to claim this hypothesis, we first confirmed the confinement of the light field at the apex of a silicon tip by means of simulations based on the finite difference time domain algorithm. An earlier report on fluorescence measurement also demonstrated light confinement at the apex of a bare silicon tip.[35] When such a bare silicon nano-tip is brought into evanescent focal spot, significant confinement of light is achieved at the apex of the tip; consequently, highly localized Raman scattering is generated from the material of the tip, i.e., from silicon. In other words, we can create a nano-light source, that emits Raman-shifted light at $520\ cm^{-1}$, with respect to the illumination wavelength. In the present experiment, we utilized this 'Raman-shifted nano-light source', and measured the transmission of this light through the sample. Since the absorption/transmission of light in graphene is directly proportional to the number of layers, and since it is much prominent than Raman scattering from graphene, an imaging process based on this absorption/transmission is expected to give

Journal of RAMAN SPECTROSCOPY

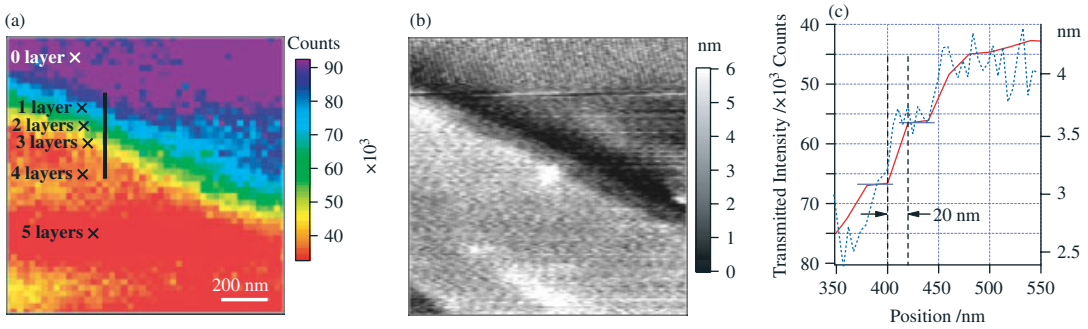

Figure 6. (a) A two-dimensional near-field optical image of ultrathin graphene sample, which is constructed by monitoring the transmitted intensity of Raman mode originating from a near-field probe made of silicon. Edge boundaries as well as variation of layer thickness can be seen at high contrast. (b) An AFM image measured from the same area of the sample, which provides a comparison with topographic image. (c) The red line indicates the line profile of the Raman intensity along the line shown in (a) and blue dotted line indicates the AFM height information at the place. The horizontal parts of this line profile correspond to the layers, while the slanted parts correspond to the edge boundaries. The spatial resolution in this image can be determined from the width of the slanted parts, which is estimated to be about 20 nm, shown by two dotted lines.

good contrast at the edge boundaries. Further, since utilization of a silicon tip provides a nano-light source that originates from highly localized area of the tip apex, an imaging based on this phenomenon would also provide high spatial resolution, corresponding to the apex of the tip. Compared to a silver-coated tip, utilizing a bare silicon tip reduces the data collection time and improves the spatial resolution in near-field measurements.

Figure 6(a) shows a two-dimensional image of the graphene sample, which was constructed by measuring the transmitted intensity of the Raman scattered signal generated at the apex of the silicon tip. The scanned area of 1.2 m × 1.2 m was measured with a resolution of 64 square pixels. The same area was also imaged with a higher resolution of 256 square pixels by AFM for the confirmation of the topography, which is shown in Fig. 6(b). Edge boundaries of graphene layers can be clearly indentified with high contrast in Fig. 6(a), which are also closely correlated with the edge boundaries in the AFM image. A comparison between two images also allows for a quantitative analysis of the layer number *n*. On the basis of the average AFM step height taken at many positions, the loss in Raman signal from the silicon tip in passing through one graphene layer is estimated to be 4.91%. One can note here that the structure of graphene is extremely thin, which essentially means that the operation of the AFM cantilever can be considered as a semi-constant height mode, and hence the topographic artifacts are negligible.[36] This estimation includes the consideration that the incident light and Raman scattering signal both experience the reduction through the highly absorbable sample and the scattering by the structure may also affect the results. We sometimes see a slight fluctuation of the silicon signal; however, on an average, the stepwise behavior at the layer edges is clear. Taking this as a calibration parameter, we estimated the number of layers from the transmitted intensity of the Raman mode originating from silicon tip. The estimated numbers of graphene layers across the sample are indicated in Fig. 6(a). This method also helped us to estimate the number of layers earlier shown in Figs. 3 and 4. As it can be seen from Fig. 6(a), the edge boundaries in this near-field image are quite sharp. In order to estimate the spatial resolution in our measurement, we examined a line profile of the near-field image across a particular step-like area, shown by the black line in Fig. 6(a). The transmitted Raman intensity along a small part of this line around one of the layer edges is shown by the red solid line in Fig. 6(c). For a comparison, the blue dotted line shows height information obtained from the AFM profile in the same part of the sample. The horizontal parts of the line profile indicate constant heights, and the slanted parts indicate the steps at the edge boundaries. The widths of these slanted parts, which should be vertical in an ideal case, give the spatial resolution in this image. As indicated by the two vertical dotted lines in Fig. 6(c), the spatial resolution in our measurement is about 20 nm.

Once we have estimated the signal reduction rate per layer, this method is robust and convenient to estimate the layer number *n* for ultrathin graphene flakes. The interlayer distance of crystalline graphite is 0.355 nm, which is quite small for an ordinary AFM system to measure with high accuracy. On the other hand, optical absorption of graphene is high enough even for a monolayer and it has a flat response in the visible range. In fact, if the area is large enough, we can even see the existence of single layer of graphene with naked eyes, which leads to the conclusion that an optical measurement is more sensitive than the AFM technique for this sample. One more advantage of the optical measurement through the transmission of silicon Raman peak is that the measurement is affected only little by the scattering from the local structures compared to the case of Rayleigh scattering. A Rayleigh scattering mapping obtained by the same experimental configuration provided only a low contrast image.

Conclusion

In conclusion, nano-scale optical analysis of *n*-graphene layers ($3 \leq n \leq 6$) was performed at high spatial resolution by TERS measurement across the layer edges that reveled nano-scale properties of the material, including the locations of the edge boundaries, the existence of local defects and local strains. The intensity change of the silicon mode coming from the tip material showed a step-like behavior across the layer boundaries, while the D-band had a slight increase of intensity at the edge boundaries. The relation between the peak shift and the line broadening for the G-band at nano-scale resolution indicated excess charge effect. The peak fluctuation of the 2D-band showed an indication of local strain distribution within the layers. Since graphene is highly absorbent in the visible range, it provided a good sample for imaging through a new near-field technique that is based on measuring the intensity of transmitted light, which in the present case was Raman scattering generated at the apex of the silicon tip. By measuring the intensity of the silicon Raman mode transmitted

through the graphene sample, we constructed a near-field image with high contrast at the edge boundary as well as with high spatial resolution of 20 nm. This technique was also used as a convenient tool to estimate the exact number of graphene layers in the sample. This new technique provides a unique possibility for high-throughput nondestructive identification of graphene layers essential for the device applications of this material.

Acknowledgements

This research has been carried out under the Program of Promotion of Environmental Improvement to Enhance Young Researchers' Independence.

References

[1] Y. Zhang, Y. W. Tan, H. L. Stormer, P. Kim, *Nature* **2005**, *438*, 201.
[2] K. S. Novoselov, A. K. Geim, S. V. Morozov, D. Jiang, M. I. Katsnelson, V. I. Grigorieva, S. V. Dubonos, A. A. Firsov, *Nature* **2005**, *438*, 197.
[3] M. A. Pimenta, M. S. Dresselhaus, L. G. Cançado, A. Jorio, R. Saito, *Phys. Chem. Chem.Phys.* **2007**, *9*, 1276.
[4] A. C. Ferrari, J. C. Meyer, V. Scardaci, C. Casiraghi, M. Lazzeri, F. Mauri, S. Piscanec, D. Jiang, K. S. Novoselov, S. Roth, A. K. Geim, *Phys. Rev. Lett.* **2006**, *97*, 187401.
[5] T. J. Echtermeyer, M. C. Lemme, J. Bolten, M. Baus, M. Ramsteiner, H. Kurz, *Eur.Phys.J. Special Topics* **2007**, *148*, 19.
[6] A. Das, S. Pisana, B. Chakraborty, S. Piscanec, S. K. Saha, U. V. Waghmare, K. S. Novoselov, H. R. Krishnamurthy, A. K. Geim, A. C. Ferrari, A. K. Sood, *Nat.Nanotech.* **2008**, *3*, 210.
[7] R. Saito, G. Dresselhaus, M. S. Dresselhaus, *Physical Properties of Carbon Nanotubes*, Imperial College Press: London, **1998**.
[8] A. K. Geim, K. S. Novoselov, *Nat. Mat.* **2006**, *6*, 183.
[9] A. Gupta, G. Chen, P. Joshi, S. Tadigadapa, P. C. Eklund, *Nano Lett.* **2006**, *6*, 2667.
[10] R. M. Stöckle, Y. D. Suh, V. Deckert, R. Zenobi, *Chem. Phys. Lett.* **2000**, *318*, 131.
[11] N. Hayazawa, Y. Inouye, Z. Sekkat, S. Kawata, *Chem. Phys. Lett.* **2001**, *335*, 369.
[12] D. S. Bulgarevich, M. Futamata, *Appl. Spectrosc.* **2004**, *58*, 757.
[13] W. H. Zhang, B. S. Yeo, T. Schmid, R. Zenobi, *J. Phys. Chem. C* **2007**, *111*, 1733.
[14] E. Bailo, V. Deckert, *Angew. Chem.* **2008**, *47*, 1658.
[15] A. Hartschuh, E. J. Sánchez, X. S. Xie, L. Novotny, *Phys. Rev. Lett.* **2003**, *90*, 095503.
[16] A. Hartschuh, H. Quiam, A. J. Meixner, N. Anderson, L. Novotny, *Nano Lett.* **2005**, *5*, 2310.
[17] N. Hayazawa, T. Yano, H. Watanabe, Y. Inouye, S. Kawata, *Chem. Phys. Lett.* **2003**, *376*, 174.
[18] T. Yano, Y. Inouye, S. Kawata, *Nano Lett.* **2006**, *6*, 1269.
[19] P. Verma, K. Yamada, H. Watanabe, Y. Inouye, S. Kawata, *Phys.Rev.B* **2006**, *73*, 045416.
[20] H. N. Zhen, T. Yu, Y. H. Lu, Y. Y. Wang, Y. P. Feng, Z. X. Shen, *ACS Nano* **2008**, *2*, 2301.
[21] Y. Saito, N. Hayazawa, H. Kataura, T. Murakami, K. Tsukagoshi, Y. Inouye, S. Kawata, *Chem. Phys. Lett.* **2005**, *410*, 136.
[22] T. Ando, *Nikkei Science* **2008**, July: 76.
[23] D. M. Basko, *Phys.Rev.B.* **2007**, *76*, 081405.
[24] L. G. Cançado, A. Reina, J. Kong, M. S. Dresselhaus, *Phys. Rev. B.* **2008**, *77*, 245408.
[25] S. Reich, C. Thomsen, *Philos.Trans.R. Soc.Lond. A* **2004**, *362*, 2271.
[26] Y. M. You, Z. H. Ni, T. Yu, Z. X. Shen, *Appl.Phys.Lett.* **2008**, *93*, 163112.
[27] E. A. Obraztsova, A. V. Osadchy, E. D. Obraztsova, S. Lefrant, I. V. Yaminsky, *Phys. Stat. Sol. B.* **2008**, *245*, 2055.
[28] P. Poncharal, A. Ayari, T. Michel, J. L. Sauvajol, *Phys.Rev.B.* **2008**, *78*, 113407.
[29] C. Casiraghi, S. Pisana, K. S. Noboselov, A. K. Geim, A. C. Ferrari, *Appl. Phys. Lett.* **2007**, *91*, 233108.
[30] M. Hulman, M. Maluska, G. Scalia, D. Obergfell, S. Roth, *Nano Lett.* **2008**, *8*, 3594.
[31] S. Pisana, M. Lazzeri, C. Casiraghi, K. Novoselov, A. K. Geim, A. C. Ferrari, F. Mauri, *Nat. Mat.* **2007**, *6*, 198.
[32] J. R. Wood, H. D. Wagner, *Appl.Phys.Lett.* **2000**, *76*, 2883.
[33] S. K. Saha, U. V. Waghmare, H. R. Krishnamurthy, A. K. Sood, *Phys. Rev. B* **2008**, *78*, 165421.
[34] R. R. Nair, P. Blake, A. N. Grigorenko, K. S. Novoselov, T. J. Booth, T. Stauber, N. M. R. Peres, A. K. Geim, *Science* **2008**, *320*, 1308.
[35] J. M. Gerton, L. A. Wade, G. A. Lessard, Z. Ma, S. R. Quake, *Phys.Rev. Lett.* **2004**, *93*, 180801.
[36] B. Hecht, H. Bielefeldt, Y. Inouye, D. Pohl, *J.Appl.Phys.* **1997**, *81*, 2492.